RSC Advances

ROYAL SOCIETY OF CHEMISTRY

www.rsc.org/advances

Synthesis of $WO_3 \cdot H_2O$ nanoparticles by pulsed plasma in liquid

Liliang Chen[a], Tsutomu Mashimo[a,*], Hiroki Okudera[b], Chihiro Iwamoto[c] and Emil Omurzak[d]

[a]Institute of Pulsed Power Science, Kumamoto University, Kumamoto 860-8555, Japan

[b]Faculty of Natural System, Institute of Science and Engineering, Kanazawa University, Kanazawa 920-1192, Japan

[f]Faculty of Engineering, Kumamoto University, Kumamoto 860-8555, Japan

[d]Priority Organization for Innovation and Excellence, Kumamoto University, Kumamoto 860-8555, Japan

*Corresponding author:

E-mail: mashimo@gpo.kumamoto-u.ac.jp;

Fax: +81 96 342 3293;

Tel: +81 96 342 3295.

Abstract

Pure orthorhombic phase $WO_3 \cdot H_2O$ nanoparticles with size of about 5 nm were synthesized by pulsed plasma in deionized water, in which tungsten metallic electrodes provides the tungsten source, the water for the oxygen and hydrogen. The quenching effect and in-liquid environment inherent in this pulsed plasma in liquid method resulted in these ultra-small particles with larger lattice expansion (a = 5.2516 Å, b = 10.4345 Å, c = 5.1380 Å), comparing with other reference lattice data. The emission lines of W I atoms, W II ions and HI atoms were observed by an optical emission spectrum to gather the information on the synthesis mechanism. These nanoparticles show higher absorption in the visible region than ST-01 TiO_2 and Wako WO_3 nanoparticles. $WO_3 \cdot H_2O$ nanoparticles displayed more activity in the photocatalytic test than commercial TiO_2 sample (ST-01). Also, the edge absorption of $WO_3 \cdot H_2O$ shifted to larger wavelength area in the UV-vis absorption pattern compared with the anhydrous tungsten oxide.

Keywords: $WO_3 \cdot H_2O$, pulsed plasma in liquid, photocatalyst, nanoparticles

Introduction

A a keen need for the new forms of green energy, the development of solar energy, for example photocatalysts, will have huge longer-term benefits, due to its affordable, inexhaustible and clean. The most used photocatalyst TiO_2 was with low efficiency to utilize the visible light[1], and many efforts to modify its band structure by doping were not so successful, because dopants usually act as recombination centers between the photogenerated electrons and holes, which reduced the photocatalytic activity greatly[2].

As a potential substitute, WO_3, which processes a small band gap of 2.4-2.8 eV, stable physicochemical properties and resilience to photocorrosion effects[3], has strong photocatalytic activity in the visible light region. However, its low conduction band level limits the photocatalysts to react with electron acceptors[4] and then increases the recombination of photogenerated electron-hole pairs. Thus many efforts were focused on the particles modified with other components, such as Ag[5,6].

Although less studied than the anhydrous tungsten oxide, the hydrate ($WO_3 \cdot H_2O$) is considered to be important to the resulting chemical properties, such as the change of optical absorption[7]. This implies the possibility of modified band structures by hydration, thus may lead to different photocatalytic properties of $WO_3 \cdot H_2O$ for some specific applications, even though the lower photocatalytic efficiency than that of WO_3.

In this study, we examined the one-step synthetic method of pulsed plasma in liquid[8,9], for the purpose to obtain $WO_3 \cdot H_2O$ nanoparticles.

1 Experimental

As shown in Figure 1, two metallic electrodes with diameter of 5 mm and 99.95% tungsten purity (Rare Metallic Co., Ltd.) were submerged in degassed deionized water without adding conducting salts (PH value is about 7) contained in a quartz beaker. Pulses with the same single-pulse duration of about 15 μs, as shown in Figure 2, were generated between the two rod tips at the voltages of 100 V and currents of 50 A, when the electrical breakdown of water happened. This process utilized deionized water to provide the oxygen and hydrogen source; tungsten metallic electrodes the tungsten. The whole synthetic system only contained the elements of W, O and H (from tungsten rods and water) without contamination from other metal cations. The microsecond duration of pulsed plasma and surrounding cool liquid helped to quench small-sized nanoparticles. After 1 hour reaction, the yellow-green nanoparticles were carefully collected after drying in air at 120 ^{o}C for 2 hours.

Nanoparticle phase purity and structure were determined by X-ray diffraction (XRD) (Rigaku RINT 2000/PC) using Cu K radiation (40 kV, 200 mA). Crystal parameters were calculated by Rietveld refinement. Morphology and microstructural characterization of prepared samples were observed by High Resolution Transmission Electron Microscopy (HRTEM) (Philips Tecnai F20). The powders for HRTEM were prepared like this: put into ethanol and deaggregated by sonication for 30 min. Optical emission spectra were obtained using an optical probe placed adjacent to the beaker and transmitting via an optical fiber to SEC2000-UV-VIS Spectrometer. HITACHI

F-2500 luminescence spectrophotometer was used to evaluate photocatalytic activity by the photodecomposition of acetaldehyde into CO_2. A Tedlar bag (AS ONE Co. Ltd.) was used as the photo-reactor vessel with a volume of 125 cm^3. 100 milligrams of $WO_3 \cdot H_2O$ powder was spread evenly on the bottom of a glass dish (area: 9.6 cm^2 = irradiation area), and the glass dish was placed in the reaction vessel described above. 500 ppm of acetaldehyde was prepared in the vessel by injection of saturated gaseous acetaldehyde. The irradiations were conducted at room temperature after equilibrium between the gaseous and adsorbed acetaldehyde had been reached, which was ascertained by monitoring the concentration by a gas chromatograph about every 30 min. The byproducts of methane and CO were negligible. The excited light source was a LED lamp with the parameters of 455 nm and 1 mW/m^2 at room temperature. And the photocatalytic results were compared with a commercial TiO_2 nanoparticle (ST-01, anatase, Ishihara Sangyo Kaisha, Ltd.) and commercial WO_3 (Wako pure chemical industries, Ltd.). UV-vis spectra of the synthesized sample, ST-01 and Wako WO_3 were taken by JASCO V-550 UV/VIS spectrometer.

2 Results and Discussion

2.1 Characterization of $WO_3 \cdot H_2O$ nanoparticles

The crystal structure of sample was check by XRD in Figure 3, in which the peaks were at 2θ = 16.5, 19.3, 23.8, 25.7, 30.5, 33.4, 34.2, 35.0, 37.7, 38.9, 42.8, 45.9, 49.2, 52.8, 54.3, 56.3, 62.8 and 66.2°, corresponding well with the 43-0679 standard card from the JCPDS. This confirmed the obtained nanoparticles were $WO_3 \cdot H_2O$, a

kind of hydrate. The absence of metallic tungsten indicated the high purity of the synthesized $WO_3 \cdot H_2O$ nanoparticles by pulsed plasma in liquid method.

Table 1 lists Rietveld refinement parameters of $WO_3 \cdot H_2O$ by pulsed plasma in deionized water, comparing with Szymanski's data[10] and reference data in PDF# 43-0679. The crystallographic structure of the synthesized $WO_3 \cdot H_2O$ sample is nicely refined using orthorhombic Pnmb space group (See Figure 4 and 5) in the region of 14-90 degrees. Observed data are indicated by dots, and the calculated profile is indicated by a solid line. Short vertical bars below the pattern represent the positions of all possible Bragg reflections, and the line below the short vertical bars represents the difference between the observed and calculated patterns. Because the hydrogen atoms were too light, they were neglected and not calculated in this refinement, just adding into the structure for imaging. Compared with other data, the crystal parameters of the prepared $WO_3 \cdot H_2O$ nanoparticles by pulsed plasma in deionized water is the largest. In our experiment, as the plasma was produced in the liquid, the oxygen source was only from the water. It was highly possible that the synthesized nanocrystals will contain oxygen vacancies which tend to increase the lattice parameters[11]. The quenching effect by the surrounding cool liquid during plasma synthesis may also help to inhibit the crystal growth resulting in lattice expansion of nanocrystals[12]. Furthermore, the a little shifted atom positions of plasma sample listed in Table 1 indicates the pulsed plasma in liquid method can introduce structure distortion in synthesized nanoparticles.

High energy density plasma commonly increases the synthesis temperature,

leading to nanoparticles growth, but low energy density plasma reduces the production rate. Thus, to optimize the balance between them, the experiment parameters, such as one pulse duration, voltage, etc., were adjusted in the experiments for the preparation of small-sized, uniform $WO_3 \cdot H_2O$ nanoparticles in a large amount. Besides, the synthetic environment of pulsed plasma in liquid method helps to disperse nanoparticles in the liquid. As shown in Figure 6, the morphology and particle size were investigated by HRTEM. The images indicated very small orthorhombic $WO_3 \cdot H_2O$ nanoparticles with the size of about 5 nm were obtained by pulsed plasma in deionized water. The calculated size according Scherer equation from the diffraction peaks of XRD patterns was about 250 um. Because we dried the particles and then take the XRD, the results here were considerable due to the aggregation of particles. The crystal parameters of $WO_3 \cdot H_2O$ are 5.238 Å×10.704 Å×5.12 Å <90.0×90.0×90.0> as shown in PDF card #43-0679. As the example shown in Figure 6a, some particles were only about 1-2 nm, thus there were only 1 or 2 unit cells in one particle. We conclude some nanoparticles were even near the unit cell level[13].

The Figure 7 shows the EDX pattern of plasma sample, in which the element Cu is due to the HRTEM grid and carbon peak sources from the membrane covered on the Cu grid. There were no extra contaminated elements. The atomic percentages of W and O were 21.06% and 78.93%, respectively, closely fitting with the ratio of these two elements in $WO_3 \cdot H_2O$, which is equal to 1:4.

2.2 Formation mechanism

The optical emission spectrum of the pulsed plasma during experiment was shown in Figure 8. And the spectral lines were identified using reference data. The coexistence of atoms W I, ions W II, and atoms H I, apparent from the optical emission spectrum, allows elucidation of the formation mechanism of the $WO_3 \cdot H_2O$ nanoparticles as follows: It's assumed that, first, very hot plasma with extreme energy ablates the tungsten metal in the rod tips to form very active tungsten atoms W I; simultaneously, the deionized water is decomposed by plasma into oxygen and hydrogen. In the plasma discharge zone, the atoms W I soon lose electrons to transform into ions W II; they then further react with oxygen and hydrogen to form a $WO_3 \cdot H_2O$ cluster in a very short time. When the clusters aggregate into crystallites and are quenched suddenly by the surrounding cool liquid, ultra-small $WO_3 \cdot H_2O$ nanoparticles appear. According to Balmer series, there will be more emission line if H-atoms exist. However, the lines at about 410 nm, 430 nm, 490 nm, were covered by the strong emission peaks of W-atoms.

2.3 Photocatalytic property and UV absorption

Until now, the photocatalytic properties of pure tungsten hydrate were not taken much attention. In these published works, most of the hydrates were mixed with other components such as WO_3 and Ag[6,14], and the researched hydrates were usually $WO_3 \cdot 0.33H_2O$ and $WO_3 \cdot 0.5H_2O$[15-17]. Only recently, Q. Zeng et al[18] reported the photocatalytic properties of pure $WO_3 \cdot H_2O$ hollow spheres. However, the synthesized

spheres only showed high photocatalytic efficiency in the acid solutions. Figure 9 shows the dependence of CO_2 evolution rate by decomposition of acetaldehyde under visible light irradiation over pure $WO_3 \cdot H_2O$ samples synthesized by pulsed plasma method upon the irradiated wavelength controlled by using various cut-off filters. The photocatalytic activity of $WO_3 \cdot H_2O$ nanoparticles by the irradiating visible light at 455 nm was higher than the commercial TiO_2 samples (ST-01) all the time. The amount of generated CO_2 for plasma sample is about 28.4% larger than ST-01 at the time of 720 min.

In order to explain the photocatalytic behavior and compare the light absorption ability, UV-vis absorption spectra (Fig. 10) were measured for $WO_3 \cdot H_2O$ nanoparticles by plasma, ST-01 and commercial wako WO_3. The obvious red shift of edge absorption and higher absorbance plot of the $WO_3 \cdot H_2O$ in the visible light region comparing with ST-01 TiO_2 sample, indicate the higher absorption, and result to better photocatalytic properties. Furthermore, the edge shift from about 440 nm for anhydrous tungsten oxide to near 480 nm for $WO_3 \cdot H_2O$ sample shows the band structure can be modified by hydration.

3 Conclusion

Pure $WO_3 \cdot H_2O$ nanoparticles were prepared in a one -step synthesis method by pulsed plasma in deionized water using two tungsten metallic rods. The lattices of the sample were expanded comparing with other reference data. This reason may due to the quenching effect by surrounding cool liquid during the preparation and the

in-liquid synthesis environment. The synthesis mechanism of the particles was analyzed using the emission spectrum. These $WO_3 \cdot H_2O$ nanoparticles, with the ultra-small particle size of about 5 nm, exhibit higher absorption than TiO_2 (ST-01) and Wako WO_3. Comparing with the anhydrous tungsten oxide, the red shift of the absorption edge in the UV-vis absorption pattern of synthesized sample by plasma indicates the possible band modification and the potential applications of the $WO_3 \cdot H_2O$ nanoparticles in the solar energy field.

Acknowledgement

This work is supported by the China Scholarship Council and the Global Center of Excellence Program of Japan.

Reference

[1] Z. Xiong, L. L. Zhang, J. Ma and X. S. Zhao, *Chem. Commun.,* 2010, **46**, 6099-6101.

[2] L. Z. Zhang, I. Djerdj, M. Cao, M. Antonietti and M. Niederberger, *Adv. Mater.,* 2007, **19**, 2083-2086.

[3] G. R. Bamwenda and H. Arakawa, *Appl. Catal. A,* 2001, **210**, 181-191.

[4] R. Abe, K. Sayama and H. Sugihara, *J. Phys. Chem. B*, 2005, **109**, 16052-16061.

[5] Z. Wang and G. Chumanov, *Adv. Mater.,* 2003, **15**, 1285-1289.

[6] P. Wang, B. Huang, X. Qin, X. Zhang Y. Dai and M. Whangbo, *Inorg. Chem.,* 2009, **48**, 10697-10702.

[7] K. O. Iwu, A. Galeckas, P. Rauwel, A. Y. Kuznetsov and T. Norby, *J. Solid State Chem.,* 2012, **185**, 245-252.

[8] E. Omurzak, J. Jasnakunov, N. Mairykova, A. Abdykerimova, A. Maatkasymova, S. Sulaimankulova, M. Matsuda, M. Nishida, H. Ihara and T. Mashimo, *J. Nanosci. Nanotechnol.,* 2007, **7**, 3157–3159.

[9] L. Chen, T. Mashimo, E. Omurzak, H. Okudera, C. Iwamoto and A. Yoshiasa, *J. Phys. Chem. C,* 2011, **115**, 9370–9375.

[10] J. T. Szymanski and A. C. Roberts, *Can. Mineral.,* 1984, **22**, 681-688.

[11] F. Zhang, S. W. Chan, J. E. Spanier, E. Apak, Q. Jin, R. D. Robinson and I. P. Herman, *Appl. Phys. Lett.,* 2002, **80**, 127-129.

[12] L. Chen, P. Fleming, V. Morris, J. D. Holmes and M. A. Morris, *J. Phys. Chem. C,* 2010, **114**, 12909-12919.

[13] E.Salje, *Acta Cryst.,* 1977, **33**, 574-577.

[14] M. S. Bazarjani, M. Hojamberdiev, K. Morita, G. Zhu, G. Cherkashinin, C. Fasel, T. Herrmann, H. Breitzke, A. Gurlo and R. Riedel, *J. Am. Chem. Soc.,* 2013, **135**, 4467-4475.

[15] L. Zou, Q. Liu, Q. Zhong, X. Bai and L. Dong, *Advanced Materials Research,* 2009, **60-61**, 480-485.

[16] X. He, C. Hu, Q. Yi, X. Wang, H. Hua and X. Li, *Catal. Lett.,* 2012, **142**, 637-645.

[17] X. Wang, X. Meng, M. Zhong, F. Wu and J. Li, *Appl. Surf. Sci.,* 2013, **282**, 826-831.

[18] Q. Zeng, Y. Zhao, J. Zhao, X. Hao, Y. Lu, J. Guo, Y. Song, F. Gao and Z. Huang, *Cryst. Res. Technol.,* 2013, **48**, 334-343.

Table

Table 1 Structure parameters of $WO_3 \cdot H_2O$ nanoparticles compared with Szymanski's and PDF#43-0679 data

Sample	Plasma sample	Szymanski's data[8]	PDF#43-0679
Space group	Pnmb	Pnmb	Pnmb
Lattice parameter			
a (Å)	5.2516(8)	5.249(2)	5.238
b (Å)	10.7345(1)	10.711(5)	10.704
c (Å)	5.1380(7)	5.133(2)	5.12
W			
position	4c	4c	4c
x	0.25	0.25	
y	0.2228(2)	0.2209(8)	
z	0.0123(2)	-0.0037(3)	
O1			
position	4c	4c	4c
x	0.25	0.25	
y	0.4293(2)	0.436(2)	
z	0.0620(9)	0.075(4)	
O2			
position	4c	4c	4c
x	0.25	0.25	
y	0.0680(2)	0.066(2)	
z	-0.0578(9)	-0.064(4)	
O3			
position	8d	8d	8d
x	0.4626(8)	0.495(8)	
y	0.2555(3)	0.227(2)	
z	0.2864(9)	0.249(5)	
Toverall	0.046758		
Profile R factors			
GOF	1.72		
Rp	14.52		
Rwp	18.32		

Figure captions

Figure 1 Schematics of system to generate pulsed plasma in deionized water by using two metallic tungsten electrodes.

Figure 2 Graph of one single pulse duration generated by the pulsed plasma in liquid system.

Figure 3 XRD powder pattern of $WO_3 \cdot H_2O$ nanoparticles by pulsed plasma in deionized water.

Figure 4 Rietveld refinement plot of $WO_3 \cdot H_2O$ nanoparticles by pulsed plasma in deionized water using orthorhombic Pnmb space group.

Figure 5 The crystal structure model of $WO_3 \cdot H_2O$ nanoparticles by pulsed plasma in deionized water.

Figure 6 High-resolution TEM images of $WO_3 \cdot H_2O$ nanoparticles by pulsed plasma in deionized water. (a) Image of one $WO_3 \cdot H_2O$ crystal with ultra-small size.

Figure 7 EDX pattern taken from the $WO_3 \cdot H_2O$ nanoparticles synthesized by pulsed plasma in deionized water in HRTEM image and the table of element content.

Figure 8 Optical emission spectrum from pulsed plasma in deionized water with tungsten electrodes.

Figure 9 Photocatalytic properties of $WO_3 \cdot H_2O$ nanocrystals grown in deionized water by pulsed plasma, comparing with a commercial TiO_2 nanoparticle (ST-01).

Figure 10 UV-vis absorption spectra of $WO_3 \cdot H_2O$ nanoparticles synthesized by pulsed plasma in deionized water comparing with commercial TiO_2 nanoparticle (ST-01) and commercial WO_3 (Wako).

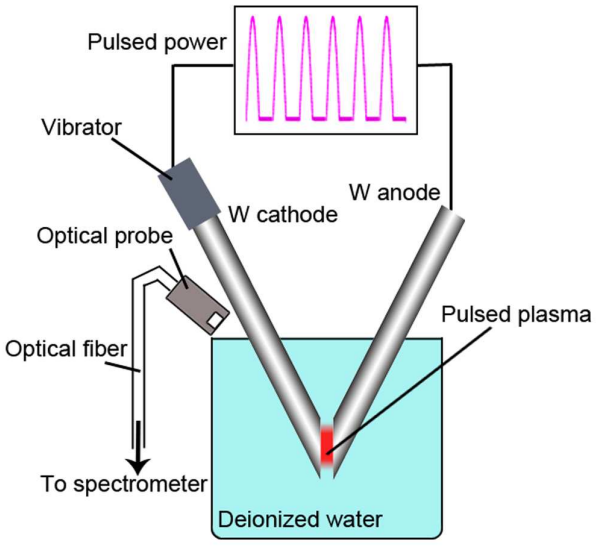

Fig. 1 Chen, et al.

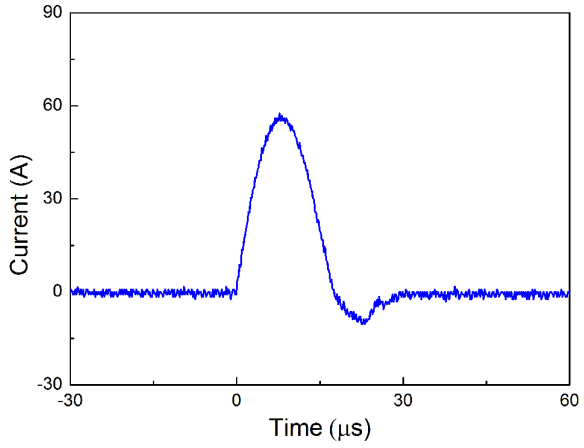

Fig. 2 Chen, et al.

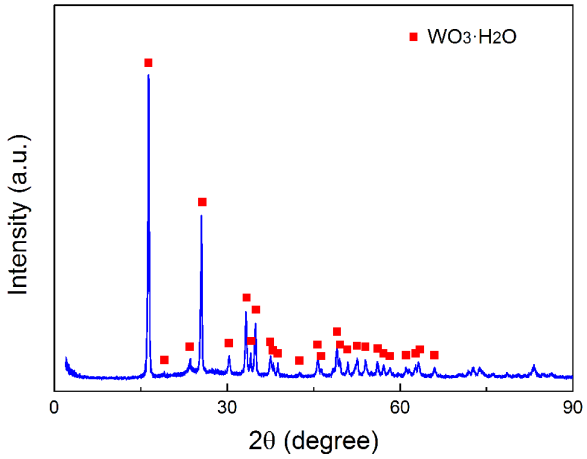

Fig. 3 Chen, et al.

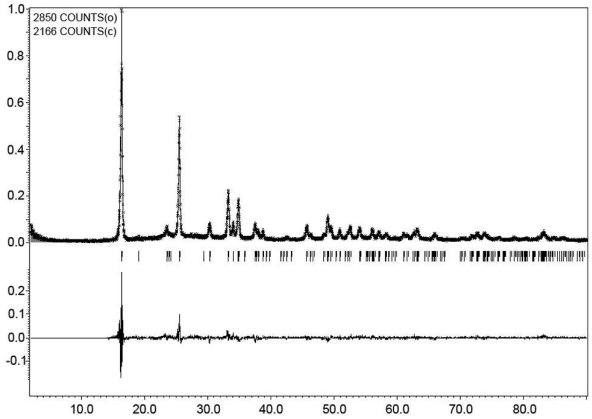

Fig. 4 Chen, et al.

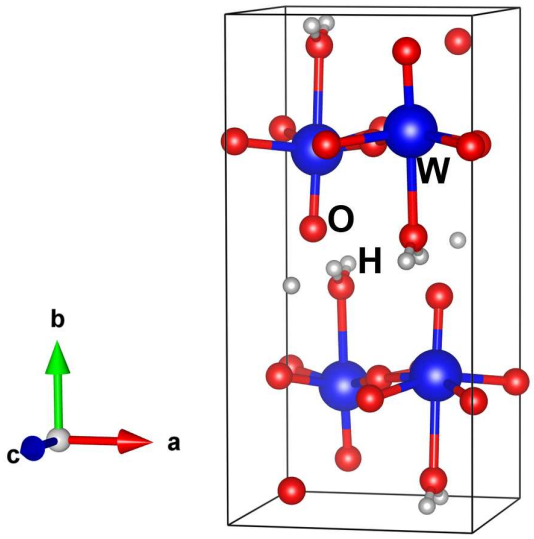

Fig. 5 Chen, et al.

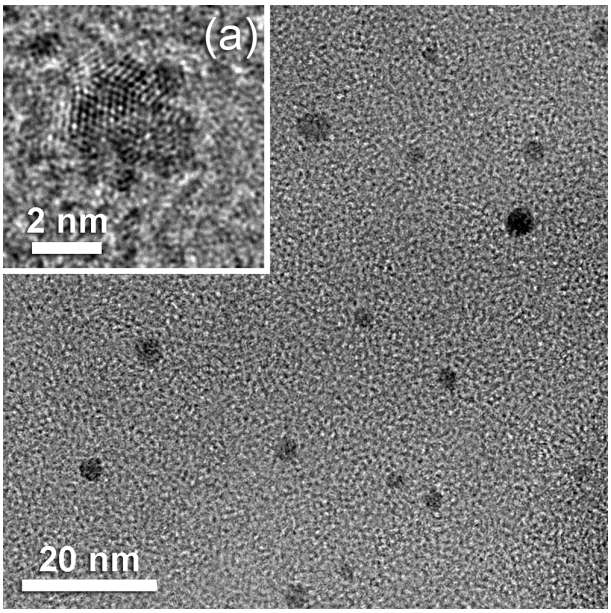

Fig. 6 Chen, et al.

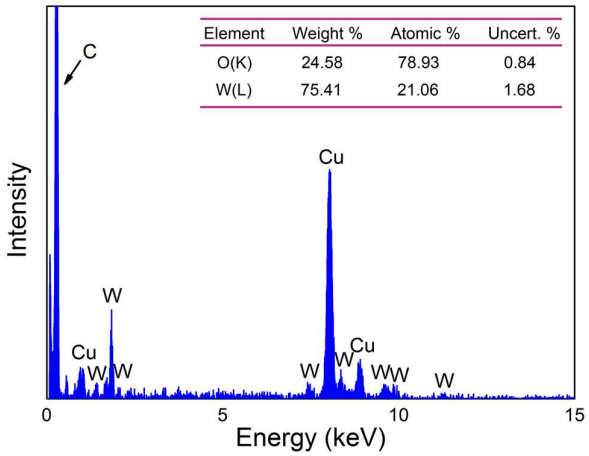

Fig. 7 Chen, et al.

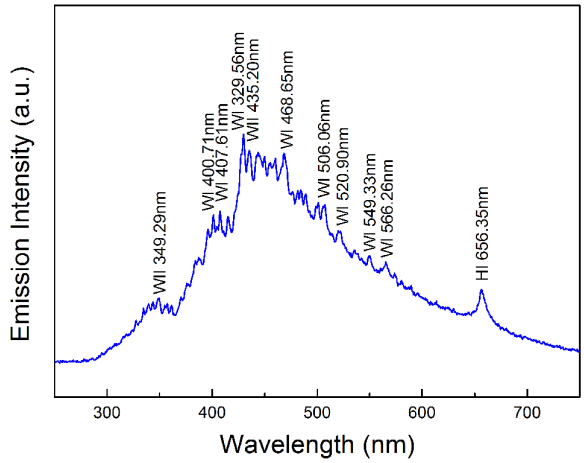

Fig. 8 Chen, et al.

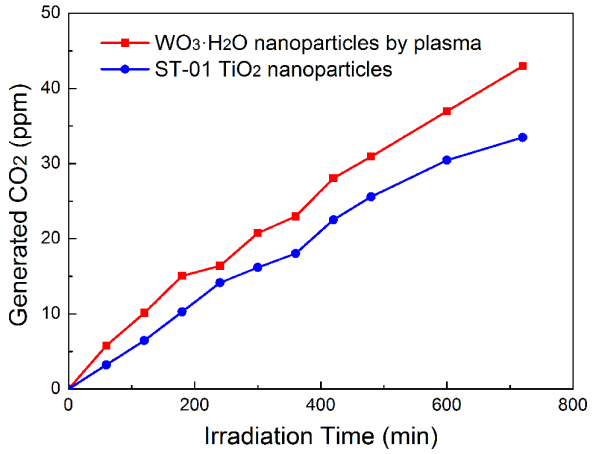

Fig. 9 Chen, et al.

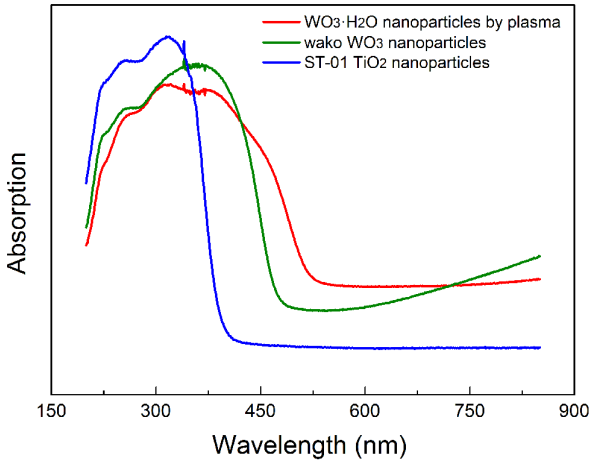

Fig. 10 Chen, et al.